PSFC/JA-97-4

Observations of Central Toroidal Rotation in ICRF Heated Alcator C-Mod Plasmas

J.E. Rice, M.J. Greenwald, I.H. Hutchinson,
E.S. Marmar, Y. Takase, S.M. Wolfe, F. Bombarda[1]

March, 1997

[1]Associazione ENEA-Euratom per la Fusione, 00044 Frascati, Italy.

Submitted to Nuclear Fusion.

This work was supported in part by the U. S. Department of Energy Contract No. DE-AC02-78ET51013.

Introduction

Rotation plays an important role in the transition from L- to H-mode [1-4]. Poloidal rotation in the edge plasma region has been closely associated with the L-H transition [5-7], and toroidal momentum confinement is well correlated with energy confinement [8-11]. While there have been several diagnostic systems designed to measure impurity toroidal rotation in tokamak plasmas [8-33], most of the observations have been made in plasmas with an external momentum source, usually provided by neutral beams. Toroidal impurity rotation in ohmic plasmas (no net momentum input) is consistent with neoclassical predictions [24,33,34]; in ohmic L-mode discharges, impurities rotate in the direction opposite to the plasma current, so in general the assumption that the majority ions and impurities (which are most often measured) rotate in the same way might be questionable [34]. In neutral beam heated plasmas, which have substantial direct momentum input, the toroidal momentum confinement time is much shorter than the neoclassical predictions [8-11]. Toroidal rotation profiles have been used to infer E_r [8,11]. In some neutral beam plasmas with ICRF heating, the rotation has been seen to drop significantly during the RF pulse [21]. Counter-current toroidal rotation associated with ion orbit loss in neutral beam and ICRF heated plasmas has been observed [26,31], and the effects of electron loss in LHCD plasmas have been seen [29]. It is difficult to separate the contribution to the rotation from the direct momentum input of the neutral beams and the rotation that may be associated with (or induced by) H-modes, although some information has been gleaned from balanced or perpendicular beam injection [8,11]. ICRF-only heated discharges provide the opportunity for the study of toroidal rotation in plasmas with no direct momentum input. Co-current rotation in ICRF-only plasmas [27,32] has been documented, alternately explained by high energy ion loss [27] and the effects of the ion pressure gradient [32], and the role of neutrals in slowing down toroidal rotation has been noted [32].

In this paper, results of impurity toroidal rotation measurements in ICRF heated Alcator C-Mod [35] plasmas are presented. The experimental setup is de-

scribed, and the magnitude and direction of the rotation are documented. Rotation time histories in a variety of different plasmas are presented, and the correlation between the velocity (momentum) increase and the plasma stored energy increase (confinement improvement) is demonstrated. Radial profiles of the rotation velocity are presented with the inferred E_r, and the decay in the velocity after the ICRF power is turned off is shown.

Experiment Description

The observations presented here were obtained from the Alcator C-Mod [35] tokamak, a compact (major radius R = 67 cm, typical minor radius of 22 cm, and $\kappa \leq 1.8$), high field device ($2.6 \leq B_T \leq 7.9$ T) which has operated with plasma currents between .23 and 1.5 MA and average electron densities between .24 and 4.4 $\times 10^{20}/m^3$. Up to 3.5 MW of ICRF power at 80 MHz [36] are available, from 2 dipole antennas, each with 0π phasing; the cases described here are all with H minority heating. During most operation, the plasma current is in the clockwise direction as viewed from the top of the machine. X-ray spectra were recorded with a spatially fixed von Hamos type crystal x-ray spectrometer [37], whose line of sight is tangent to the plasma axis, pointing in the counter clockwise direction, as seen from above, and a vertically scannable von Hamos type x-ray spectrometer array [38]. The array consists of five spectrometers, two of which are scanable in a vertical plane oriented 6° off of a major radius, directed at the plasma axis, in a slight counter clockwise view. The other three spectrometers have a similar slight (6°) clockwise view. The spectrometer layout with respect to Alcator C-Mod is shown in Fig.1. Rotation velocities have been determined from the Doppler shifts of the Ar^{17+} Lyman α doublet [39,40] (1s $^1S_{\frac{1}{2}}$ - 2p $^2P_{\frac{3}{2}}$ at 3731.12 mÅ, and 1s $^1S_{\frac{1}{2}}$ - 2p $^2P_{\frac{1}{2}}$ at 3736.53 mÅ), and the Ar^{16+} forbidden line, z [41,42] (1s2p $^3S_1$ -$1s^2$ $^1S_0$ at 3994.28 mÅ). The forbidden line in the heliumlike argon spectrum is utilized for the Doppler shift measurement instead of the (usually) brighter resonance line because there is no contamination from nearby unresolved high n satellites which

can give rise to an apparent shift due to changes in relative intensity [19]. Spectra are typically collected every 20-50 ms during plasma discharges. Argon is routinely injected into Alcator C-Mod plasmas through a piezoelectric valve, to provide x-ray transitions for Doppler width ion temperature measurements [43]. Absolute wavelength calibration for the tangentially viewing spectrometer was obtained from the potassium K_α lines generated from a KCl fluorescence x-ray source [40]. There was no wavelength calibration for the spectrometer array viewing at $\pm 6°$, so for those measurements all velocities are relative to the pre-RF conditions.

Observations of Toroidal Rotation and Scalings

Shown in Fig.2 are x-ray spectra including the hydrogenlike argon doublet employed for the rotation analysis, obtained using the tangentially viewing spectrometer from a 0.8 MA discharge with the current in the clockwise direction. The thin vertical lines indicate the rest wavelengths. The spectrum shown by the dash-dot-dot-dot line is from the ohmic portion; during the steady state period of ohmic L-mode discharges, the rotation velocities are typically small (in the counter-current direction), and there is little shift [33]. Shown by the solid line in the figure is a spectrum taken during the H-mode phase of the same discharge, induced by 2 MW of ICRF power. The two spectra have been normalized in intensity to emphasize the wavelength shift. Since the spectrometer was viewing tangentially counter clockwise, and the solid spectrum is blue-shifted, the argon is rotating clockwise, in same direction as the plasma current during the RF pulse. This is in the direction opposite to the rotation of impurities in ohmic L-mode plasmas [8,24,33,34]. The magnitude of the shift is $\sim$.5 mÅ, which yields a toroidal rotation velocity of (.5 mÅ/3731.1 mÅ) $\times$ c = 4.0 $\times$ 10^6 cm/s, in the co-current direction. Since the major radius of Alcator C-Mod is 67 cm, this corresponds to an angular rotation speed of 60 kRad/sec.

The toroidal rotation may also be determined from the heliumlike argon forbid-

den line. Shown in Fig.3a and 3b are spectra recorded from a spectrometer viewing the plasma mid-plane, at an angle of 6° from a major radius, in a slight counter clockwise view. The spectra of Fig.3a were obtained from a 1.1 MA discharge (clockwise current), and there is a blue-shift of .13±.01 mÅ during the H-mode phase (solid spectrum), when the plasma stored energy increased by .12 MJ. This corresponds to a toroidal rotation velocity increase of (.13 mÅ/3994.3 mÅ)/sin(6°) $\times$ c = 1.0 $\times$ 10^7 cm/s (150 kRad/sec), in the co-current direction. The spectra of Fig.3b were obtained with the same view from a 1.0 MA discharge with the plasma current in the counter clockwise direction, and there is a red-shift of .07±.01 mÅ during the 2.7 MW ICRF pulse, indicating that the argon is rotating in the counter clockwise direction, again co-current. This L-mode discharge had a stored energy increase of 45 kJ, when the magnitude of the toroidal rotation velocity increased by 5.3 $\times$ 10^6 cm/s, and still opposite to the rotation direction in ohmic discharges. The phasing of the RF antennas for this case was the same as in Fig.3a. Shown in Fig.3c are spectra recorded from a 6° clockwise view from a 0.8 MA discharge with the plasma current in the clockwise direction, and there is a red-shift of .08±.01 mÅ during the 2.7 MW ICRF pulse, indicating that the argon is rotating at 6.0 $\times$ 10^6 cm/s, in the co-current clockwise direction. The line of sight of the spectrometer used for this measurement was also pointing 8 cm below the plasma midplane for this discharge, and could therefore be sensitive to a poloidal component of the rotation. However, for this same discharge, the spectrometer with a 6° counter clockwise toroidal view was also pointed 8 cm below the midplane and recorded an equal and opposite line shift, indicating that any poloidal component to the rotation velocity is $\leq$ 3$\times$$10^5$ cm/s (the detection limit) at this radius. The widths of the lines in the solid (ICRF) spectra are broader due to a simultaneous increase in the ion temperature, and the intensities of the lines in the ohmic and ICRF cases have been normalized in order to emphasize the wavelength shift.

The time histories of several parameters of interest for a 5.4 T, 0.82 MA deuterium L-mode plasma are shown in Fig.4. Argon is injected in a 50 ms wide pulse at .3 s into the discharge, and the subsequent central argon density ($\times$ 10^4), along

with the central electron density, is shown in frame (b). The impurity content α, defined as $n_I\ Z_I^2/n_i\ Z_i^2$ (where I denotes impurity and i denotes majority ion), is everywhere less than 0.06 for this discharge. The RF turns on at 0.54 s (d), and there is a subsequent increase in the electron and ion temperatures (c), and a very modest increase in the stored energy (a). This L-mode plasma also begins to rotate in the co-current direction at about 1.5×10^6 cm/s, as shown in the bottom frame. This plasma briefly enters H-mode after 1.2 s, as evident in the drop of the D_α signal (e), and increases in the stored energy and the electron and argon densities. There is also a slight increase in the rotation velocity. The time histories of these same parameters for a 5.3 T, 0.82 MA deuterium H-mode plasma are shown in Fig.5. In this case there is a dramatic increase in the stored energy of 75 kJ when the plasma enters H-mode ($\sim$ .68 s), and the central rotation velocity reaches over 1.0×10^7 cm/s. The rotation velocity increases over a time period of 100 ms or so after the H-mode begins, indicating that the toroidal rotation is a consequence of the H-mode transition, and not something which triggers it. There are also substantial increases in the electron and argon densities, and in the electron and ion temperatures during the same time. Another H-mode discharge is shown in Fig.6; in this case the plasma enters H-mode at .6 s when the D_α drops, and the stored energy, rotation velocity, and densities and temperatures all increase. This plasma returns to L-mode at .75 s (when the RF power decreased by a factor of 2). The stored energy, electron density and rotation velocity all then approach their previous L-mode values, while the electron and ion temperatures remain elevated. This suggests a correlation between the rotation velocity increase and the stored energy increase, and not just in the ion temperature or gradient.

This correlation is demonstrated in Fig.7; there is a general increase in the impurity toroidal rotation velocity increase during the ICRF pulse and the stored energy increase, over nearly two orders of magnitude, although stored energy increases less than 5 kJ are difficult to measure. This data set includes a range of RF powers between .5 and 3.1 MW, central electron densities between 0.9 and 5.9 $\times 10^{20}/m^3$, plasma currents between 0.6 and 1.2 MA, and clockwise and reverse

currents, in both L- and H-mode plasmas, with H-factors between .75 and 2.3. The points shown as asterisks (diamonds) were from H-mode (L-mode) plasmas, and the four points shown as 'plus signs' were obtained from purely ohmic H-mode discharges, which also rotate in the co-current direction after the plasma undergoes the L-H transition. The points shown as triangles were from reversed current discharges (rotating in the opposite direction as the other points in the figure, but still co-current), which had substantial stored energy and rotation velocity increases, but were not strict H-mode plasmas because of the absence of any drop in D_α emission. While there is a distinct correlation, especially for large stored energy increases, some of the points are somewhat far from the main trend. The three points surrounded by boxes were from H-mode discharges which had high levels of D_α radiation (enhanced D_α discharges [44,45]), and don't rotate as fast as otherwise similar discharges, an effect which has also been seen in JET [32] plasmas. The points shown as thin diamonds, which seem to be rotating rather quickly for such a small stored energy increase, were from one particular L-mode run which had a peculiar argon density time history. One of these discharges is shown in Fig.8; in this case the argon density, which is around $2 \times 10^{16}/\mathrm{m}^3$ before the ICRF pulse, drops over a factor of two when the RF turns on, and the plasma begins rotating in the co-current direction at 2×10^6 cm/s. At this time there is also an increase in the electron density, and electron and ion temperatures, but only a slight increase in the stored energy. Although the argon ions are rotating relatively quickly for this modest stored energy increase, there are fewer of them so the total argon momentum increase is not so large. This suggests that perhaps a quantity of interest for comparison with the stored energy increase is the increase in the argon momentum or angular momentum density. The quantity $\Delta(n_{Ar}V_{Tor})$, which is proportional to both the argon momentum density ($n_{Ar}m_{Ar}V_{Tor}$) and to the argon angular momentum density ($n_{Ar}m_{Ar}V_{Tor}R$), is plotted as a function of the stored energy increase in Fig.9. The main difference between this figure and Fig.7 is that the points from the falling argon density run (c.f. Fig.8) are now closer to the main group of points. The overall scatter in the points has slightly

increased but the trend for the highest rotation points persists. Attemps to find a correlation between the rotation velocity increase and other parameters such as the RF power, ion temperature or ion pressure increase have resulted in very large scatter in the data points, with no suggestive trends resulting. The fact remains that the plasmas with the highest rotation velocities generally have the best energy confinement. This is emphasized in Fig.10 where the ITER-89P H-factor [46] is plotted as a function of rotation velocity increase. Plasmas which rotate the fastest have the highest H-factors. There is a continuous range of L- and H-mode behavior presented here; some of the high H-factor L-mode plasmas rotate more quickly than the lower H-factor H-mode plasmas, and there is no sharp dichotomy. The purely ohmic H-mode points, from rather unspectacular 0.6 MA, 3.4 T discharges, are shown by the diamonds.

Rotation Velocity Profiles and E_r

Some radial profile information on the rotation velocity is available from vertical scans of the spectrometer array. Two of the spectrometers were scanned on a shot-to-shot basis during three very similar 5.4 T, 0.8 MA deuterium H-mode discharges, that had stored energy increases of 75 kJ during the 2.0 MW ICRF pulses. Shown in Fig.11 is the radial profile of the toroidal rotation velocity; the velocity is highest in the plasma center, and rapidly falls off with minor radius. For these plasmas the last closed flux surface on the midplane was at 20.5 cm. The asterisks are from the spectrometer with a 6° counter clockwise view, and the spectral lines were blue-shifted in this case; the boxes are from the spectrometer with a 6° clockwise view, and the lines were red-shifted (see Fig.3). For the two points near 5.5 cm, both spectrometers were viewing at nearly the same *poloidal* angle. Since the wavelength shift was equal in magnitude at this radius, but opposite in sign, and the two spectrometers had opposite *toroidal* views, the rotation at this radius must mostly be toroidal, with an upper limit for the poloidal component $\leq 3\times10^5$ cm/s. For the point at 9.1 cm, the signal level before the H-mode was very low, and there is

a large error in the pre-RF rotation velocity (as in Fig.3c). At this radius, in this case, it's not possible to make a statement about any poloidal component in the velocity. The rotation velocity decrease with radius has been seen in many neutral beam heated plasmas [8,9,11,23,30], and has been predicted from theory for TFTR plasmas ('self-generated' rotation) [3].

An independent measurement of central plasma rotation has been obtained from the frequency of the sawtooth precursors, which are large during H-mode, and can be observed both with the fast ECE temperature measurements and via magnetic perturbation (Mirnov) coils outside the plasma. From the frequency of these $n = 1$ modes an equivalent velocity is deduced, which is taken to be toroidal although the measurement itself cannot distinguish between toroidal and poloidal rotation. Typically, the velocity rises rapidly from a low value before the plasma enters H-mode and peaks about 0.1 s later, settling thereafter to a steady state level about 10 - 20% less than its peak. Its direction is co-current, the same as the argon. The point at 9.5 cm in Fig.11 shows a solid vertical error bar indicating the range of observed mode velocities for the shots in this series. The associated horizontal error bar indicates the range of uncertainty of the midplane sawtooth inversion radius deduced from the ECE.

The theoretical rotation velocity [47] of the sawtooth precursor relative to the frame in which $E_r = 0$ may be between the electron diamagnetic velocity if the mode is resistive, and half the ion diamagnetic velocity if the mode is ideal. One may then deduce a velocity of the argon ions, which are essentially at rest in the $E_r = 0$ frame, as will be demonstrated below. The argon velocity deduced depends on what is assumed about this theoretical relative velocity. The dotted error bar in Fig.11 shows the range of corresponding argon velocities obtained from the extremes of the relative mode rotation assumption.

An estimate of the contribution to E_r from the toroidal rotation, or the required E_r needed to give rise to the toroidal rotation can be made from the force balance equation:

$$E_r = \nabla P/neZ + V_{Tor}B_P - V_{Pol}B_T. \quad (1)$$

The quantity V_{Tor} B_P for argon as a function of minor radius is shown in Fig.12 for the rotation profile of Fig.11, where the poloidal magnetic field has been computed from EFIT [48]. The equivalent E_r is nearly 300 V/cm at r/a = .3. For comparison, the negative of the ion diamagnetic term, $-\nabla P_i/(e\ n_i)$, is also shown, calculated from the measured ion temperature profile and computed ion density profile, and is everywhere a factor of two smaller. The Ar^{16+} diamagnetic contribution, $\nabla P_{Ar^{16+}}/(16\ e\ n_{Ar^{16+}})$, calculated from the measured ion temperature profile and the measured Ar^{16+} density profile (also shown negative in the figure) is negligible, and the argon poloidal rotation term has been ignored inside of r/a = .3. Similar E_r profiles have been deduced in PBX-M neutral beam heated discharges [11]. From Eq.(1) the ion (deuteron) rotation velocity may be estimated; the electric field has been determined from the argon toroidal rotation (Fig.12). Ignoring ion poloidal rotation near the center, the ion toroidal rotation velocity is larger by the ion diamagnetic term, and so the ions rotate about 50% faster than the argon ions, inside r/a = .3. If the ions are rotating at 1.5×10^7 cm/s, then they are carrying 700 A/cm^2, about half the central current density. Conversely, the electrons rotate about 50% slower than the argon, because of the negative charge in the diamagnetic term.

Since there is negligible momentum input from ICRF waves launched with 0π phasing and therefore the input torque is unknown, it is not possible to calculate the momentum confinement time directly during the ICRF pulse. From the decay in the rotation velocity after the ICRF heating is turned off, an estimate for the central momentum confinement may be derived. Shown in Fig.13 is the time history of the rotation velocity near the end of the ICRF heating pulse; the toroidal rotation decays with a 1/e time of 68 ms, a value close to the energy confinement time of 52 ms. This is much faster than the 3 seconds predicted for the neoclassical toroidal rotation damping time from Eq.(36) in Ref.[49]. The observed decay time and the

spin-up time at the beginning of the ICRF heating pulse are similar (and similar with the rise and decay of the stored energy, Fig.5), which suggests that the central toroidal rotation is a consequence of the H-mode, and not something which triggers the transition.

Conclusions

The central impurity toroidal rotation has been measured from the Doppler shift of x-ray lines from argon in Alcator C-Mod ICRF heated plasmas. During the ICRF pulse, and in the absence of direct momentum input, the rotation is in the co-current direction (opposite to that during the ohmic portion). The mechanism for this rotation remains obscure. When the plasma current direction is reversed, the rotation during ICRF heating also switches, maintaining the co-current direction. The magnitude of the rotation is largest ($\sim$1.3 $\times$ 10^7 cm/s, 200 kRad/s) during the best H-mode discharges. The magnitude of the rotation velocity during ICRF heating increases with the stored energy increase, regardless of input power or electron density, over a range of two orders of magnitude. Some of the lowest stored energy increase L-mode discharges had relatively high argon rotation velocities, but accompanied by a substantial decrease in the argon density, suggesting a possible correlation between the plasma stored energy increase and the argon (angular) momentum density increase. There are also some discharges, which had a large stored energy increase with very modest rotation velocity increase, that also had greater D_α emission during the H-mode phase, suggesting that a higher edge neutral density may hinder the rotation. Certainly the plasmas with the highest H-factors rotate the fastest. In general, the rotation is not an effect only of H-mode per se; some high H-factor L-mode plasmas rotate faster than some modest H-factor H-mode plasmas. Co-current rotation has also been observed during purely ohmic H-modes. The toroidal rotation velocity is peaked at the magnetic axis, and falls off quickly with minor radius. There is no evidence for a poloidal component of the rotation velocity inside of 6 cm. Values of E_r up to 300 V/cm at r/a = .3 have been

inferred. The rotation velocity decays with a characteristic time between 50 and 100 ms after the ICRF is turned off, comparable to the energy confinement time, and much shorter than the predicted neoclassical momentum slowing down time.

Acknowledgements

The authors would like to thank K. Burrell, P. Diamond, S. Migliuolo and J. Goetz for helpful discussions, J. Terry for D_α measurements, J. Irby for electron density measurements, A. Hubbard and P. O'Shea for electron temperature measurements, C. Fiore for ion temperature measurements, Y. Wang for argon density profiles and the Alcator C-Mod operations and RF groups for expert running of the tokamak. Work supported at MIT by DoE Contract No. DE-AC02-78ET51013.

References

[1] K.C.Shiang and E.C.Crume, Phys. Rev. Lett. **63** (1989) 2369.

[2] K.H.Burrell et al., in *Plasma Physics and Controlled Nuclear Fusion Research 1994* Proceedings of the 15th International Conference, Seville, Spain, Vol.1 (IAEA, Vienna 1996) 221.

[3] P.H.Diamond et al., in *Plasma Physics and Controlled Nuclear Fusion Research 1994* Proceedings of the 15th International Conference, Seville, Spain, Vol.3 (IAEA, Vienna 1996) 323.

[4] R.A. Moyer et al., Phys. Plasmas **2** (1995) 2397.

[5] R.J.Groebner et al., Phys. Rev. Lett. **64** (1990) 3015.

[6] F.Wagner et al., in *Plasma Physics and Controlled Nuclear Fusion Research 1990* Proceedings of the 13th International Conference, Wahington D.C., Vol.1 (IAEA, Vienna 1991) 277.

[7] Y.Miura et al., in *Plasma Physics and Controlled Nuclear Fusion Research 1990* Proceedings of the 13th International Conference, Wahington D.C., Vol.1 (IAEA, Vienna 1991) 325.

[8] S.Suckewer et al., Nucl. Fusion **21** (1981) 1301.

[9] K.H.Burrell et al., Nucl. Fusion **28** (1988) 3.

[10] A.Kallenbach et al., Plasma Phys. Contr. Fusion **33** (1991) 595.

[11] N.Asakura et al., Nucl. Fusion **33** (1993) 1165.

[12] M.G.Bell, Nucl. Fusion **19** (1979) 33.

[13] S.Yamamoto et al., in *Plasma Physics and Controlled Nuclear Fusion Research 1982* Proceedings of the 9th International Conference, Baltimore, MD, Vol.1 (IAEA, Vienna 1983) 73.

[14] R.C.Isler et al., Appl. Phys. Lett. **42** (1983) 355.

[15] C.A.Kostek et al., Plasma Phys. **25** (1983) 421.

[16] K.Brau et al., Nucl. Fusion **23** (1983) 1643.

[17] V.I.Bugarya et al., Nucl. Fusion **25** (1985) 1707.

[18] N.C.Hawkes and N.J.Peacock, Nucl. Fusion **25** (1985) 971.

[19] M.Bitter et al., Phys. Rev. A **32** (1985) 3011.

[20] R.C.Isler et al., Nucl. Fusion **26** (1986) 391.

[21] M. Mattioli et al., J. Appl. Phys. **64** (1988) 3345.

[22] R.Bartiromo et al., Rev. Sci. Instrum. **60** (1989) 237.

[23] H.Weisen et al., Nucl. Fusion **29** (1989) 2187.

[24] W.A.Peebles et al., in *Plasma Physics and Controlled Nuclear Fusion Research 1990* Proceedings of the 13th International Conference, Wahington D.C., Vol.1 (IAEA, Vienna 1991) 589.

[25] S.D.Scott et al., Phys. Rev. Lett **64** (1990) 531.

[26] K. Ida et al., Nucl. Fusion **31** (1991) 943.

[27] L.-G.Eriksson et al., Plasma Phys. Contr. Fusion **34** (1992) 863.

[28] B.P. Duval, B. Joye and B. Marchal, Nucl. Fusion **32** (1992) 1405.

[29] Y.Koide et al., in *Plasma Physics and Controlled Nuclear Fusion Research 1992* Proceedings of the 14th International Conference, Wurzburg, Vol.1 (IAEA, Vienna 1993) 777.

[30] K. Nagashima et al., Nucl. Fusion **34** (1994) 449.

[31] H.Hsuan et al., in *Proceedings of the 11th Topical Conference on Radio-Frequency Power in Plasmas*, Palm Springs, CA 1995, AIP Conference Proceedings 355 (Editors: Ronald Prater, Vincent S. Chan) American Institute of Physics, Woodbury, New York 1996 p. 39

[32] L.-G.Eriksson et al., Plasma Phys. Contr. Fusion **39** (1997) 27.

[33] J.E.Rice et al., Nucl. Fusion **37** (1997) 421.

[34] Y.B.Kim, P.H.Diamond and R.J.Groebner, Phys. Fluids B **3** (1991) 2050.

[35] I.H.Hutchinson et al., Phys. Plasmas **1** (1994) 1511.

[36] S.N.Golovato, M. Porkolab, Y. Takase et al., in *Proceedings of the 11th Topical Conference on Radio-Frequency Power in Plasmas*, Palm Springs, CA 1995, AIP Conference Proceedings 355 (Editors: Ronald Prater, Vincent S. Chan) American Institute of Physics, Woodbury, New York 1996 p.23

[37] E.Källne, J.Källne, E.S.Marmar and J.E.Rice, Phys. Scr. **31** (1985) 551.

[38] J.E.Rice et al., Rev. Sci. Instrum. **61** (1990) 2753.

[39] G. W. Erickson, J. Phys. Chem. Ref. Data **6** (1977) 831.

[40] E.S.Marmar et al., Phys. Rev. A **33** (1986) 774.

[41] L. A. Vainshtein and U. I. Safronova, Physica Scripta **31** (1985) 519.

[42] J.E.Rice et al., Phys Rev A **35** (1987) 3033.

[43] J.E.Rice et al., Rev. Sci. Instrum. **66** (1995) 752.

[44] M. Greenwald et al., Nucl. Fusion **37** (1997) xxx.

[45] Y. Takase, R. Boivin, F. Bombarda, P.T. Bonoli, C. Fiore, et al. "High Power Density H-Modes in Alcator C-Mod," paper F1-CN-64/A5-4 in Proceedings of the 16th IAEA Fusion Energy Conference, Montreal, October 1996 (International Atomic Energy Agency, Vienna, in press).

[46] P. Yushmanov, T. Takizuka, K. Riedel, O. Kardaun, J. Cordey, S. Kaye, D. Post, Nucl. Fus. 30, (1990) 1999.

[47] S. Migliuolo, Nucl. Fusion, 33 (1993) 1721.

[48] L. L. Lao et al., Nucl. Fusion **25** (1985) 1611.

[49] J.W.Connor et al., Plasma Phys. Contr. Fusion **29** (1987) 919.

Figure Captions

Fig. 1 Experimental layout.

Fig. 2 X-ray spectra of the Ar^{17+} Ly_α doublet for the ohmic (dash-dot-dot-dot) and ICRF (solid) portions of a 0.8 MA clockwise current discharge with 2 MW of ICRF power. The Ly_α rest wavelengths are shown by the thin vertical lines.

Fig. 3 X-ray spectra of the Ar^{16+} forbidden line for the ohmic (dash-dot-dot-dot) and ICRF (solid) portions of a.) a 1.1 MA clockwise current discharge with 2 MW of ICRF power and 6° counter clockwise view, b.) a 1.0 MA counter clockwise current discharge with 2.7 MW of ICRF power and 6° counter clockwise view, and c.) a 0.8 MA clockwise current discharge with 2.7 MW of ICRF power and 6° clockwise view.

Fig. 4 The time histories of several parameters for a 5.4 T, deuterium L-mode discharge. In the top frame (a) is the plasma stored energy. In the second frame (b) are the central electron density (solid) and the central argon density (dash-dot-dot-dot, $\times 10^4$). In the third frame (c) are the central electron temperature (with sawteeth) and the central ion temperature (smooth). In frame (d) is the ICRF power and in frame (e) is the D_α emission. In the bottom frame (f) is the central toroidal rotation velocity of argon ions, and typical error bars are shown.

Fig. 5 The time histories of several parameters for a 5.3 T, deuterium H-mode discharge. The legend is the same as in Fig.4.

Fig. 6 The time histories of several parameters for a 5.4 T, deuterium H-mode discharge. The legend is the same as in Fig.4.

Fig. 7 The toroidal rotation velocity increase during the ICRF pulse as a function of the plasma stored energy increase in H-mode (L-mode) discharges are shown as

asterisks (diamonds). The points shown as triangles are from plasmas with reversed current. The points shown as asterisks surrounded by boxes are from high D_α H-mode discharges, as light diamonds from falling argon density shots, and as plus signs from ohmic H-mode discharges.

Fig. 8 The time histories of several parameters for a 5.4 T, deuterium L-mode discharge. The legend is the same as in Fig.4.

Fig. 9 The increase in the product $n_{Ar}V_{Tor}$ (proportional to the argon (angular) momentum density increase) as a function of plasma stored energy increase.

Fig. 10 The H-factor as a function of toroidal rotation velocity increase. The points shown as diamonds are from ohmic H-mode discharges.

Fig. 11 The toroidal rotation velocity as a function radius for three identical H-mode discharges. The points shown by asterisks are from a counter clockwise view; the points shown by boxes are from a clockwise view. The point at 9.5 cm is the sawtooth precursor rotation velocity.

Fig. 12 The inferred E_r, from the observed argon toroidal rotation velocity profile and the computed poloidal magnetic field, as a function of minor radius. Shown by the smooth curve is the negative of the ion (deuteron) diamagnetic term calculated from the measured ion pressure gradient, and by the dash-dot-dot-dot curve is the negative of the Ar^{16+} diamagnetic term.

Fig. 13 The decay of the toroidal rotation velocity after the ICRF pulse is turned off, for an H-mode discharge. The solid line is the best fit exponential decay, and the RF pulse, which peaks at 2 MW, is shown by the thin line.

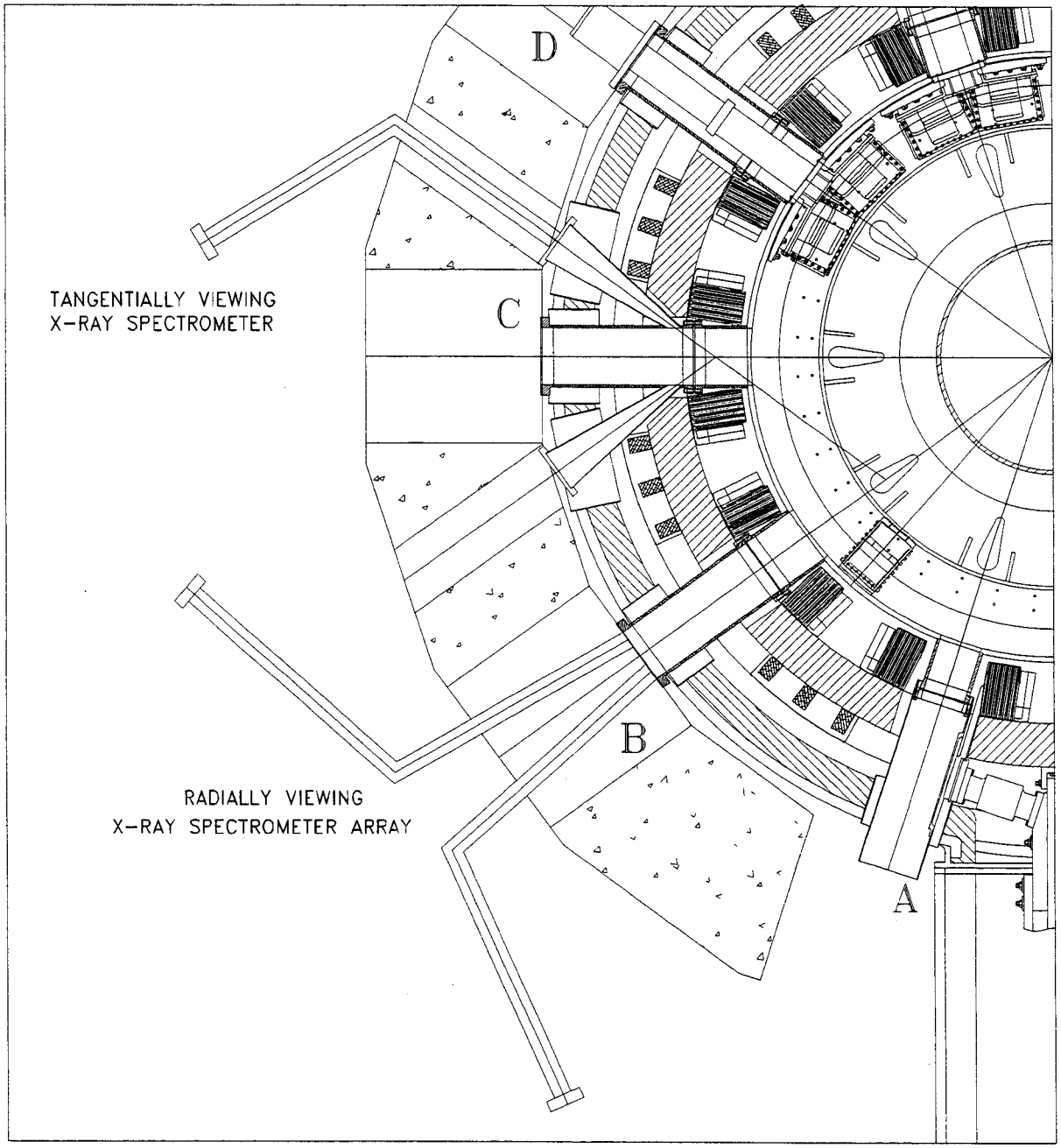
D
TANGENTIALLY VIEWING
X-RAY SPECTROMETER
C
B
RADIALLY VIEWING
X-RAY SPECTROMETER ARRAY
A

Figure 1

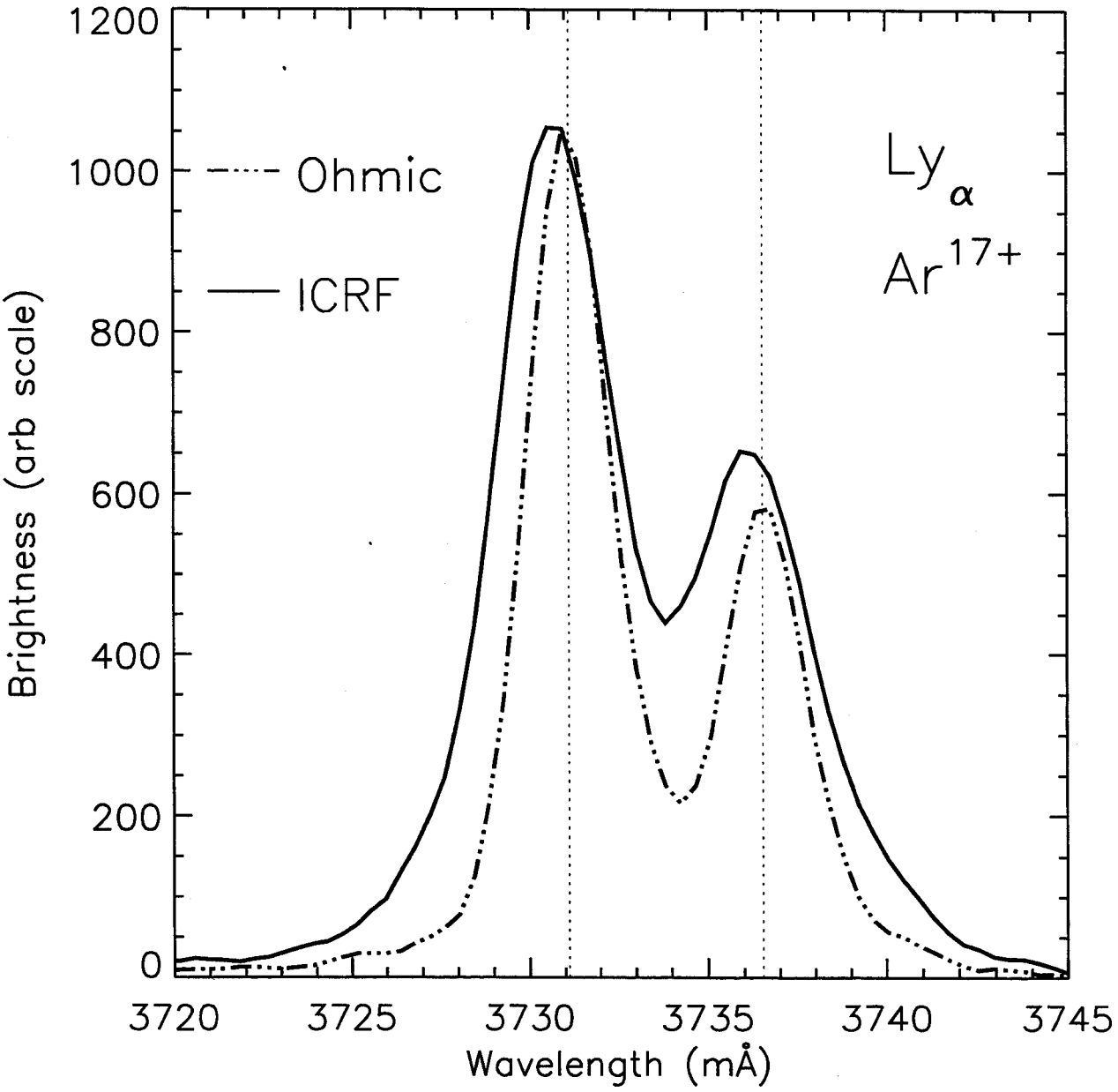
1200
1000
800
600
400
200
0
Brightness (arb scale)
Ohmic
ICRF
Ly α
Ar 17+
3720
3725
3730
3735
3740
3745
Wavelength (mÅ)

Figure 2

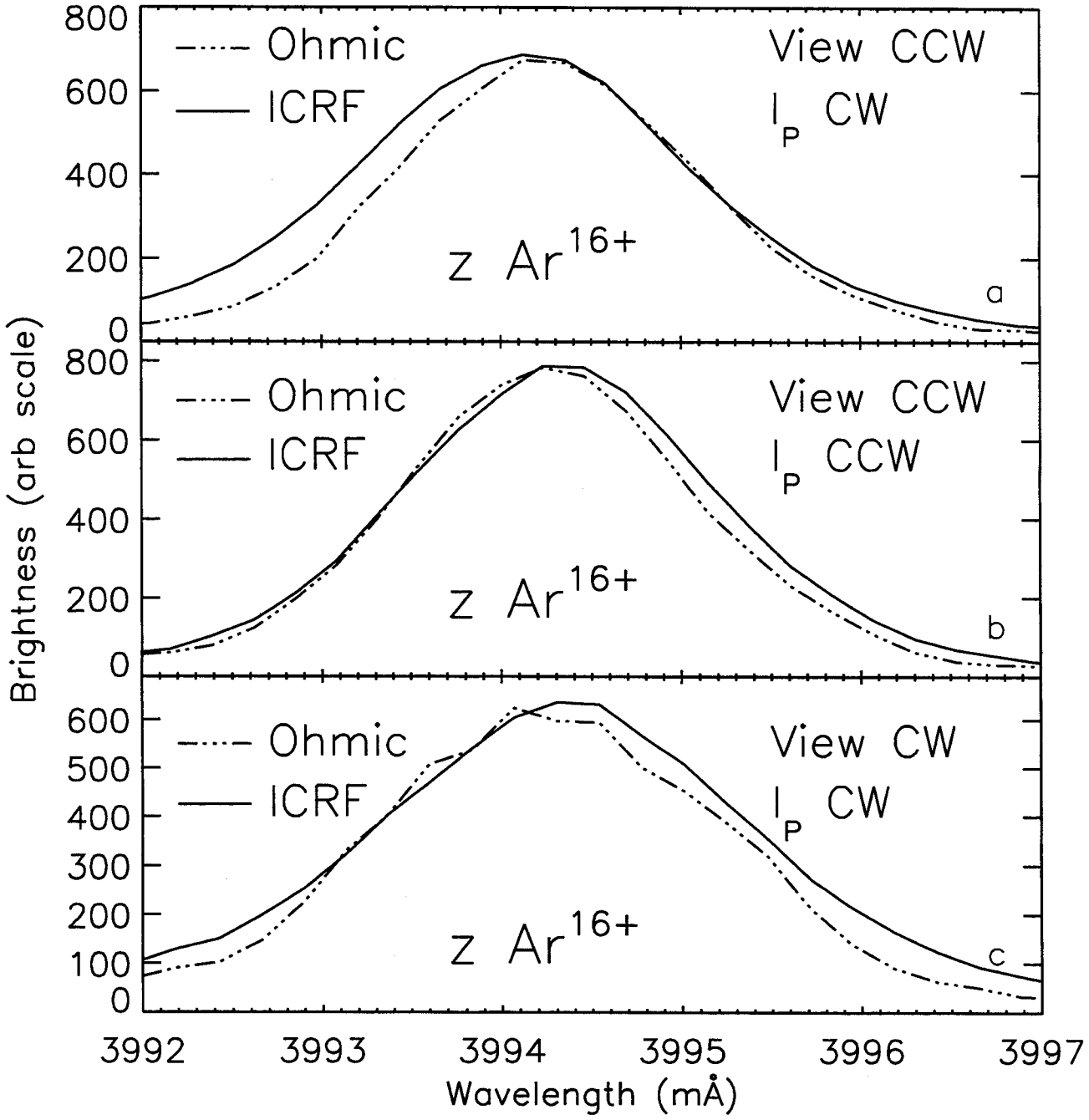
Ohmic
ICRF
View CCW
I_P CW
z Ar^{16+}
a
Ohmic
ICRF
View CCW
I_P CCW
z Ar^{16+}
b
Ohmic
ICRF
View CW
I_P CW
z Ar^{16+}
c
Brightness (arb scale)
Wavelength (mÅ)
3992
3993
3994
3995
3996
3997

Figure 3

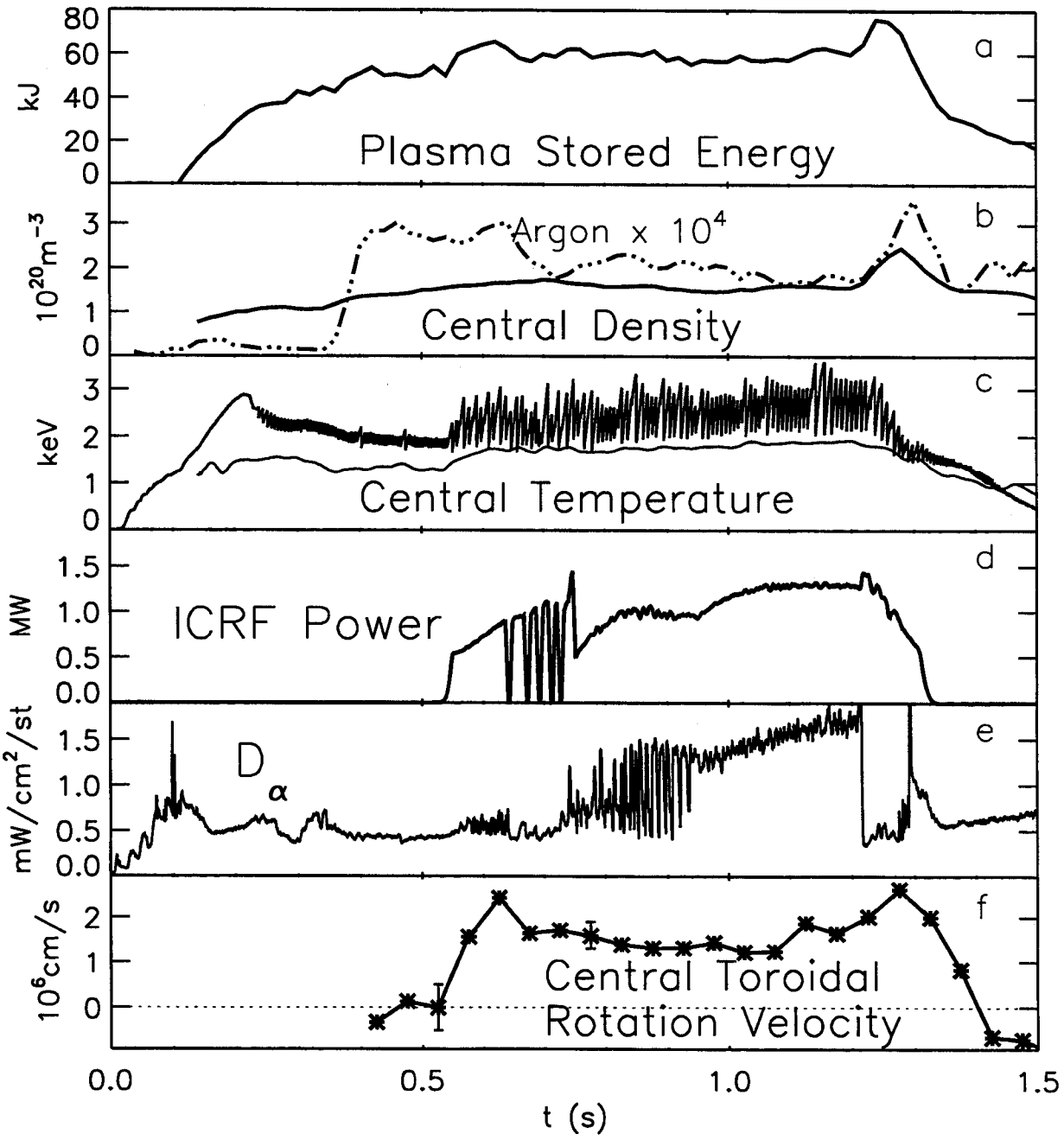
80
60
40
20
0
kJ
Plasma Stored Energy
a
3
2
1
0
$10^{20}m^{-3}$
Argon x 10^4
Central Density
b
3
2
1
0
keV
Central Temperature
c
1.5
1.0
0.5
0.0
MW
ICRF Power
d
1.5
1.0
0.5
0.0
$mW/cm^2/st$
D_α
e
2
1
0
$10^6cm/s$
Central Toroidal
Rotation Velocity
f
0.0
0.5
1.0
1.5
t (s)

Figure 4

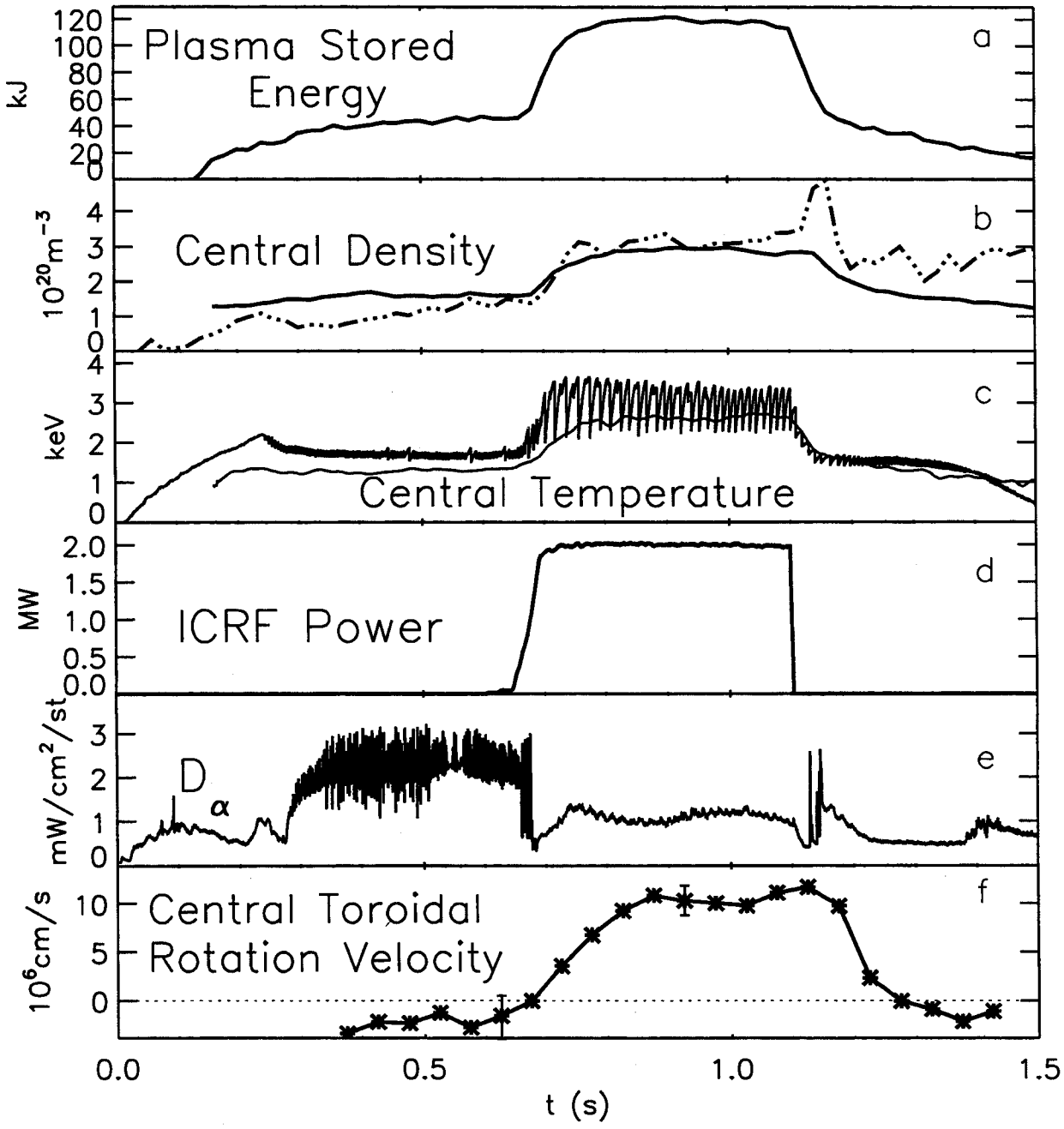
Plasma Stored Energy
a
kJ
120
100
80
60
40
20
0
Central Density
b
$10^{20}m^{-3}$
4
3
2
1
0
Central Temperature
c
keV
4
3
2
1
0
ICRF Power
d
MW
2.0
1.5
1.0
0.5
0.0
D_α
e
$mW/cm^2/st$
3
2
1
0
Central Toroidal Rotation Velocity
f
$10^6 cm/s$
10
5
0
0.0
0.5
1.0
1.5
t (s)

Figure 5

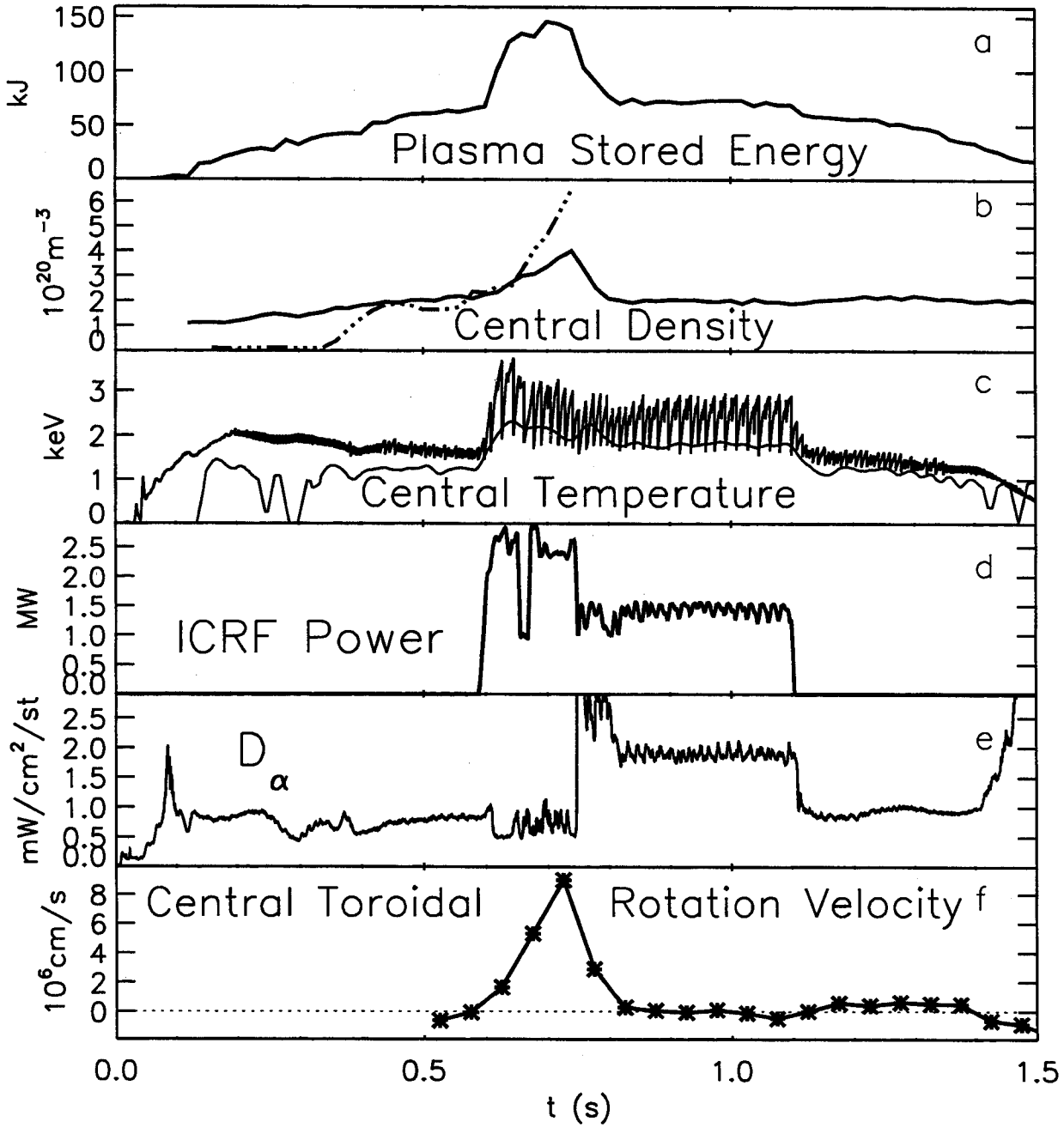
150
100
50
0
kJ
a
Plasma Stored Energy
6
5
4
3
2
1
0
$10^{20}m^{-3}$
b
Central Density
3
2
1
0
keV
c
Central Temperature
2.5
2.0
1.5
1.0
0.5
0.0
MW
d
ICRF Power
2.5
2.0
1.5
1.0
0.5
0.0
$mW/cm^2/st$
D_α
e
8
6
4
2
0
$10^6cm/s$
Central Toroidal Rotation Velocity
f
0.0
0.5
1.0
1.5
t (s)

Figure 6

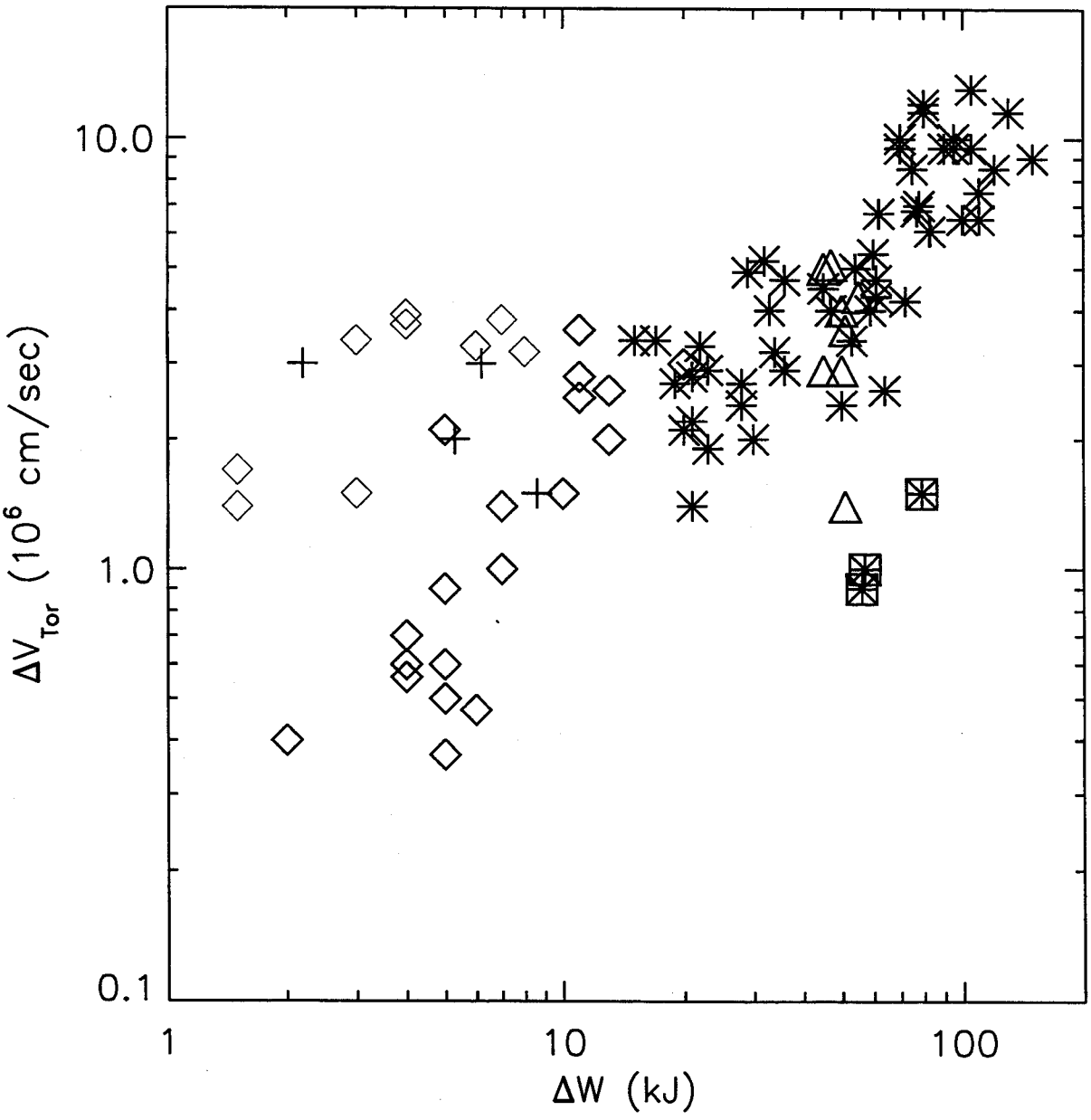

Figure 7

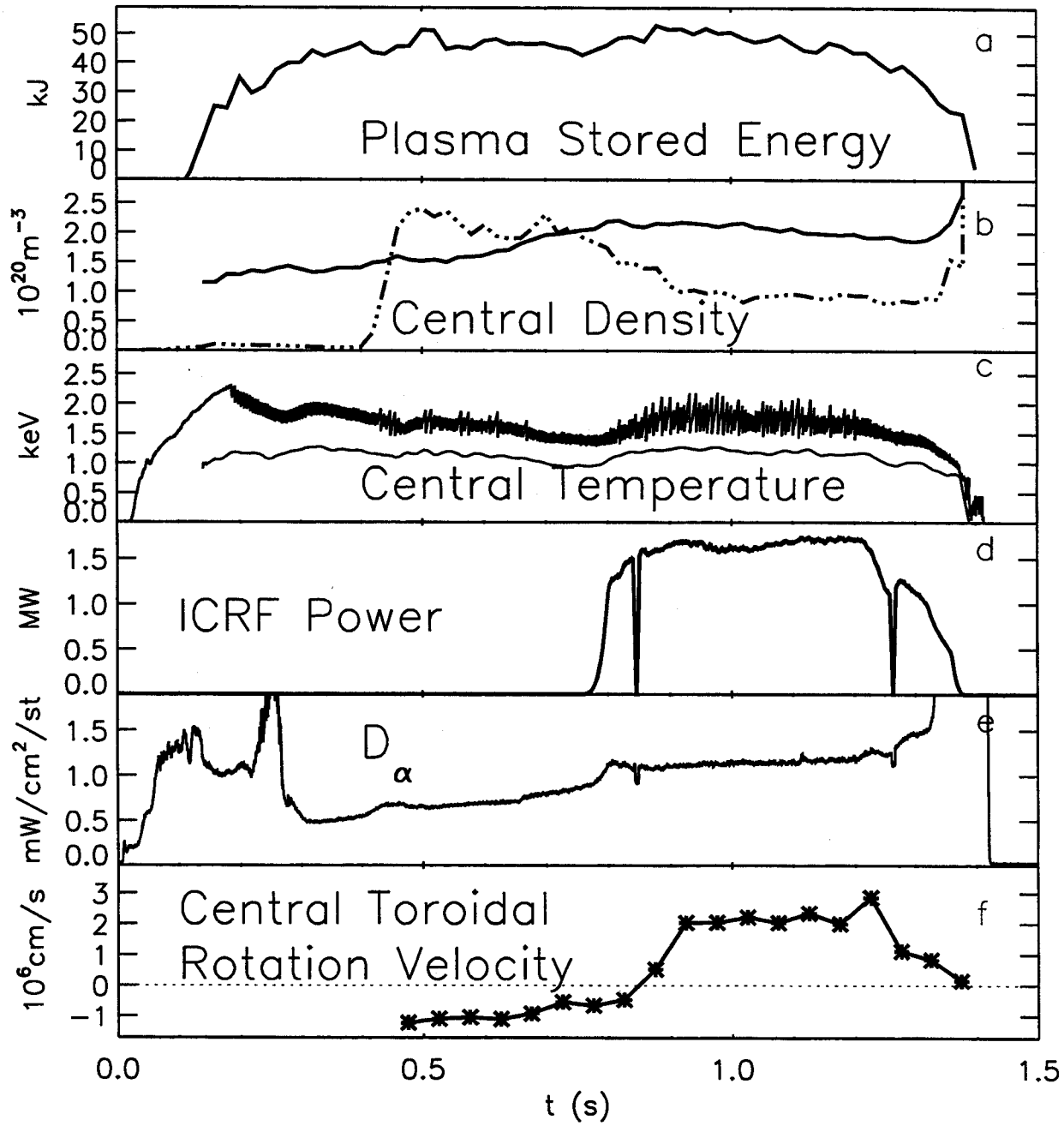
a
Plasma Stored Energy
kJ
50
40
30
20
10
0
b
Central Density
$10^{20}m^{-3}$
2.5
2.0
1.5
1.0
0.5
0.0
c
Central Temperature
keV
2.5
2.0
1.5
1.0
0.5
0.0
d
ICRF Power
MW
1.5
1.0
0.5
0.0
e
D_α
$mW/cm^2/st$
1.5
1.0
0.5
0.0
f
Central Toroidal
Rotation Velocity
$10^6cm/s$
3
2
1
0
−1
0.0
0.5
1.0
1.5
t (s)

Figure 8

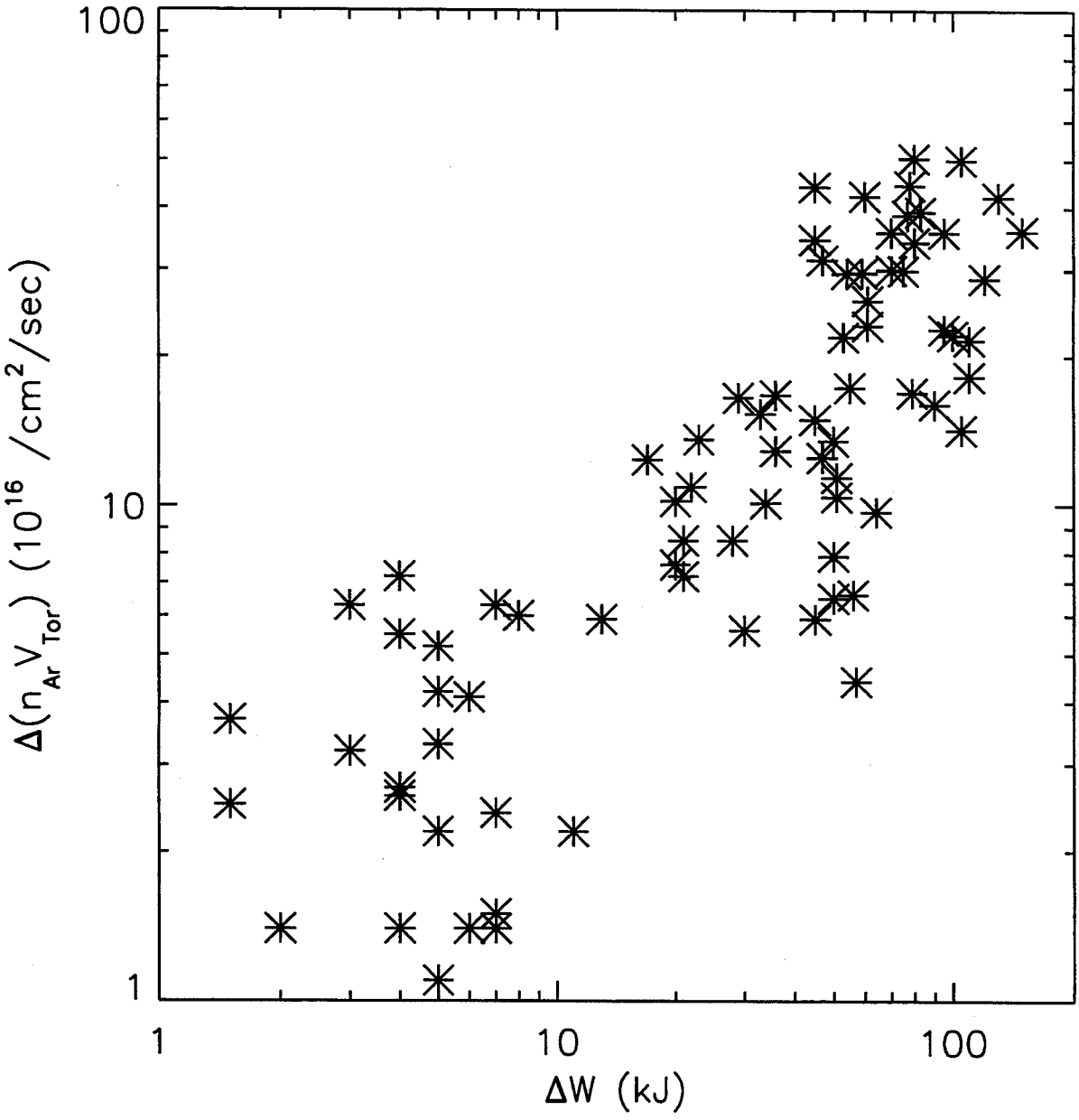

Figure 9

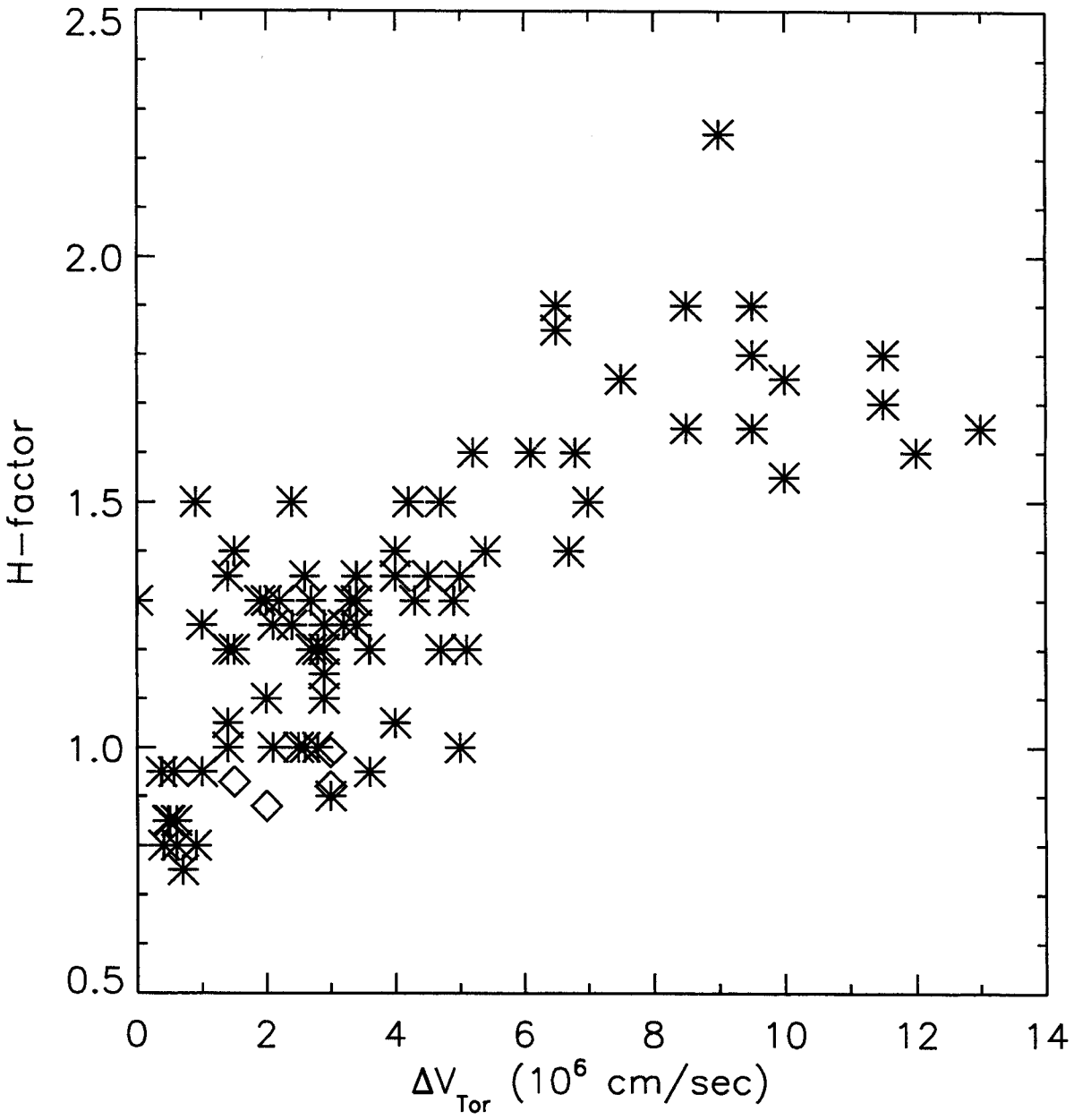

Figure 10

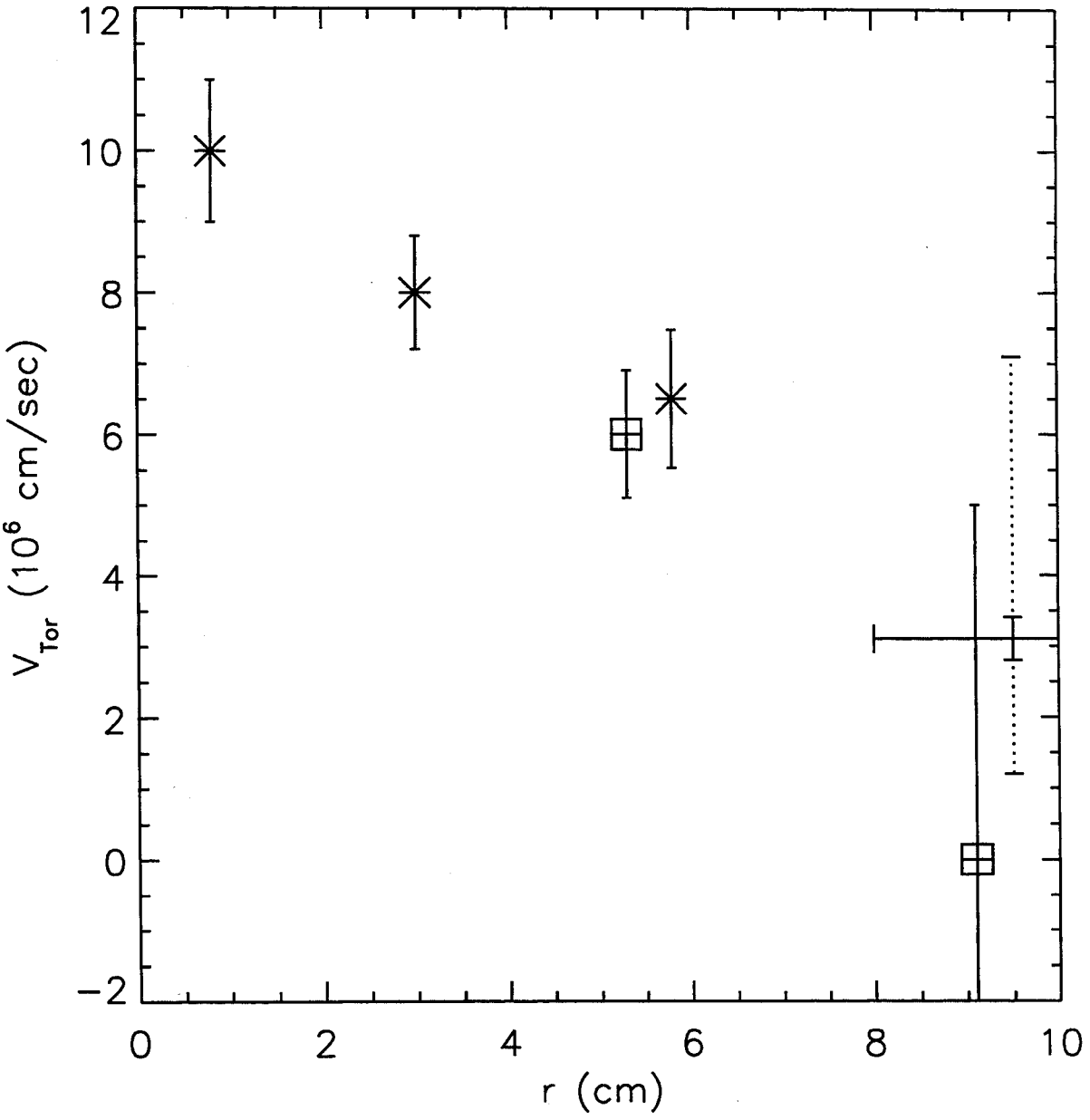

Figure 11

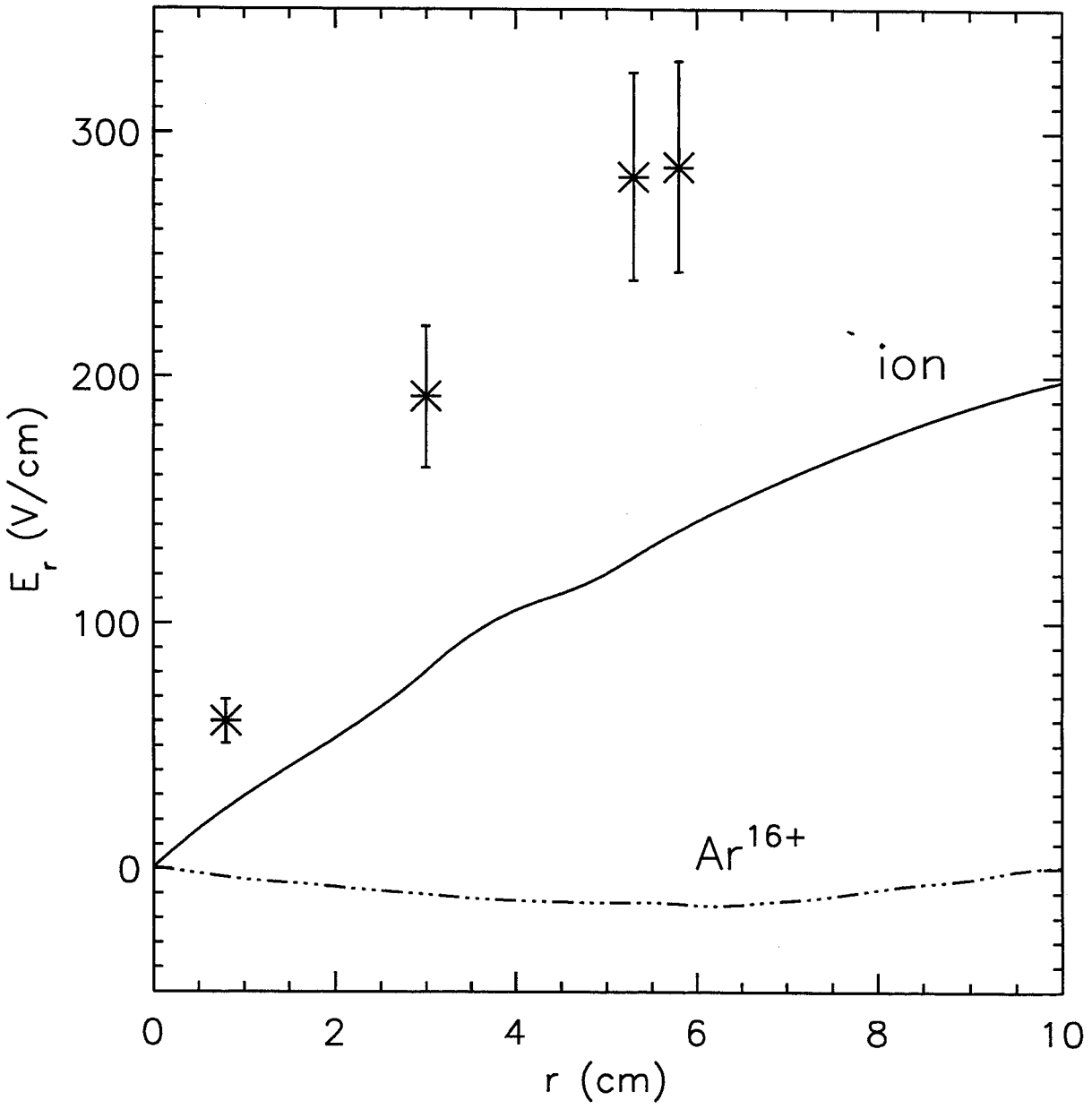

Figure 12

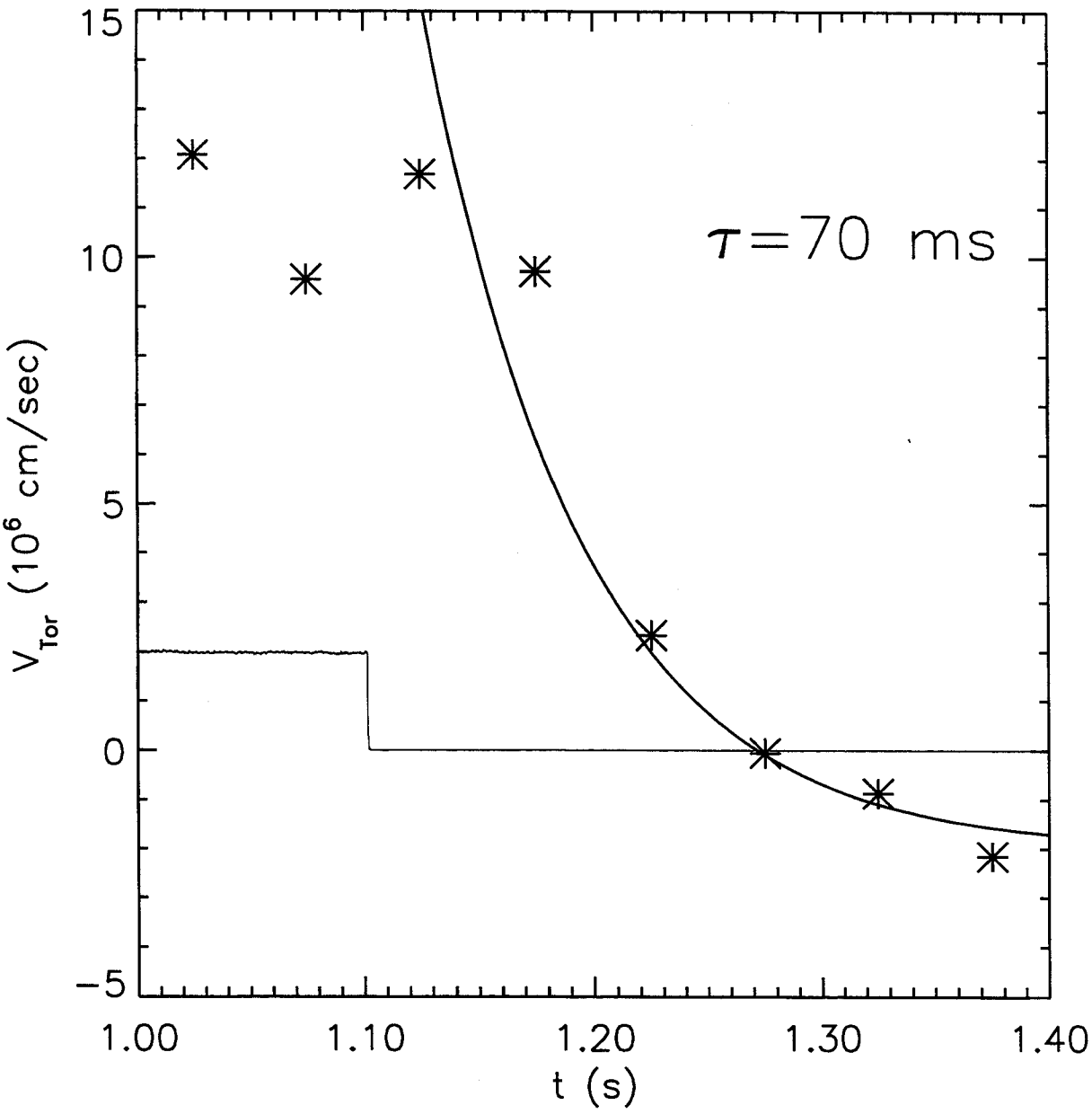

Figure 13